

This fast switching (~ 10 ns) occurs at very high current densities ($> 10^6$ A/cm²). The nonbolometric signal had a rise time of ~ 4 ns and a fall time of ~ 5 to 6 ns and its amplitude is a function of the laser fluence.

The bolometric response was simulated by a 1-D heat-propagation model in conjunction with an electrical model describing the electrical response of the film. The results of the simulation were in agreement with the thermal component of the observed signal. The dependence of response time of the simulated signal on initial temperature, bias current, and the laser fluence are consistent with our experimental observations.

ACKNOWLEDGMENT

This work was supported by the National Science Foundation Grant No. DMR-8913524 and by the Laser Fusion Feasibility Project at the Laboratory for Laser Energetics, which is sponsored by the New York State Energy Research and Development Authority and the University of Rochester.

REFERENCES

1. A. Frenkel *et al.*, J. Appl. Phys. **67**, 3054 (1990).
2. W. R. Donaldson, A. M. Kadin, P. H. Ballentine, and R. Sobolewski, Appl. Phys. Lett. **54**, 2470 (1989).
3. J. E. Zimmerman *et al.*, Appl. Phys. Lett. **51**, 617 (1987).
4. R. H. Koch *et al.*, Appl. Phys. Lett. **51**, 200 (1987).
5. M. K. Kelly *et al.*, Appl. Phys. Lett. **53**, 2333 (1988).
6. Y. Enomoto and T. Murakami, J. Appl. Phys. **59**, 3807 (1986).
7. H. S. Kwok *et al.*, Appl. Phys. Lett. **54**, 2473 (1989).
8. M. Johnson, Appl. Phys. Lett. **59**, 1371 (1991).
9. P. H. Ballentine *et al.*, J. Vac. Sci. Technol. A **9**, 1118 (1991).
10. P. H. Ballentine, A. M. Kadin, M. A. Fisher, D. S. Mallory, and W. R. Donaldson, IEEE Trans. Magn. **25**, 950 (1989).
11. C. Uher and A. B. Kaiser, Phys. Rev. B **36**, 5680 (1987).

2.B High-Reflectance Transport-Mirror Development for the OMEGA Upgrade

The transport mirrors that will direct each of the 60 laser beams toward the target chamber are of critical importance to the OMEGA Upgrade. These mirrors, made of complex multilayer coatings, must withstand the full fluence of the OMEGA laser after it has been converted from 1054 nm to 351 nm. This article summarizes the requirements for the mirrors, describes the development procedure and results, proposes a mechanism for the observed damage, and provides a solution for the OMEGA Upgrade configuration.

The high incidence angles required for the transport mirrors have proven to be an important parameter in the study of how the mirrors damage. Initial work established designs, materials, and processes that would meet requirements at normal incidence. However, the mirrors must operate over a wide range of incidence angles and incident polarizations. Designs that work well at normal incidence must be changed for oblique incidence and optimized for a given polarization. Materials differ in their damage characteristics at high incidence angles depending on the type of defect in the film. Substrate preparation and cleaning play a large role in damage of the mirror and can produce large variations in damage thresholds in a series of otherwise identical substrates.

The transport-mirror configuration for the OMEGA Upgrade was changed from a three-mirror to a two-mirror configuration in 1991. This change was made to reduce the effects of stimulated rotational Raman scattering (SRRS) on the beams by reducing the optical path length from the frequency-conversion crystals to the target. One result was an increase in the average angle of incidence on the mirrors (see Fig. 51.14). We will show later that, in general, the laser-damage threshold of the mirror decreases with incidence angle.

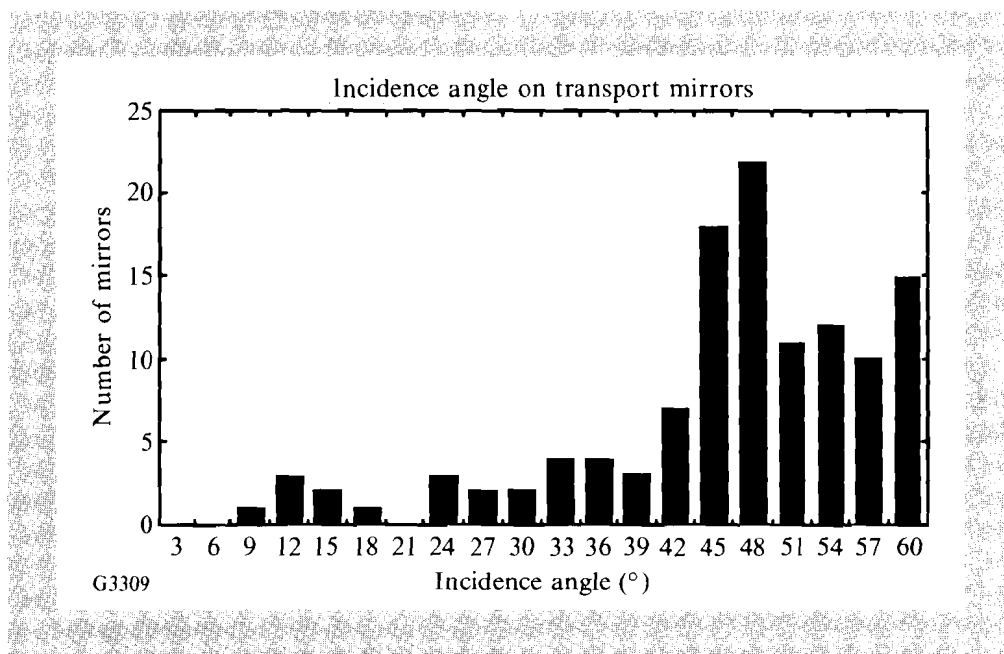


Fig. 51.14

The two-mirror transport scheme for the OMEGA Upgrade yields a high-average-incidence angle. This histogram shows that most mirrors will see an incidence angle between 40° and 60° and more than half of the mirrors will see an incidence angle greater than 47° .

The transport mirrors must reflect 351 nm efficiently without damaging. The reflectance should be higher than 99.5% regardless of incident angle and polarization. The peak fluence of the 351-nm light incident on any optic at this stage in the laser will be 2.8 J/cm^2 for the 0.7-ns main pulse. A second foot pulse will propagate within the annular main pulse with a pulse width five to ten times that of the main pulse. A conservative fourth-root temporal scaling law was used to design fluence loading of the foot pulse under the assumption that the coating would survive the main pulse. The mirrors will also be subjected to unconverted 1054-nm (1ω) and 527-nm (2ω) light. This light also must not damage the coating or the underlying substrate.

Summary of Results for Normal Incidence

Transport mirror coating materials and designs were first evaluated at normal incidence to facilitate both fabrication and testing.¹ The mirrors use two dielectric materials coated in a sequence of layers, which causes constructive interference in the Fresnel reflection from the interfaces. The designs may require more than 30 layers to achieve the required reflectance. Designs are grouped into categories by the dielectric materials used for the layers. A coating design (layer sequence and thickness), the materials, the process used to create the coating, and the substrate are referred to as a high-reflector (HR) system. The results at normal incidence were encouraging and provided several material combinations and process conditions that improved the measured damage threshold beyond the state of the art. In summary the results indicated

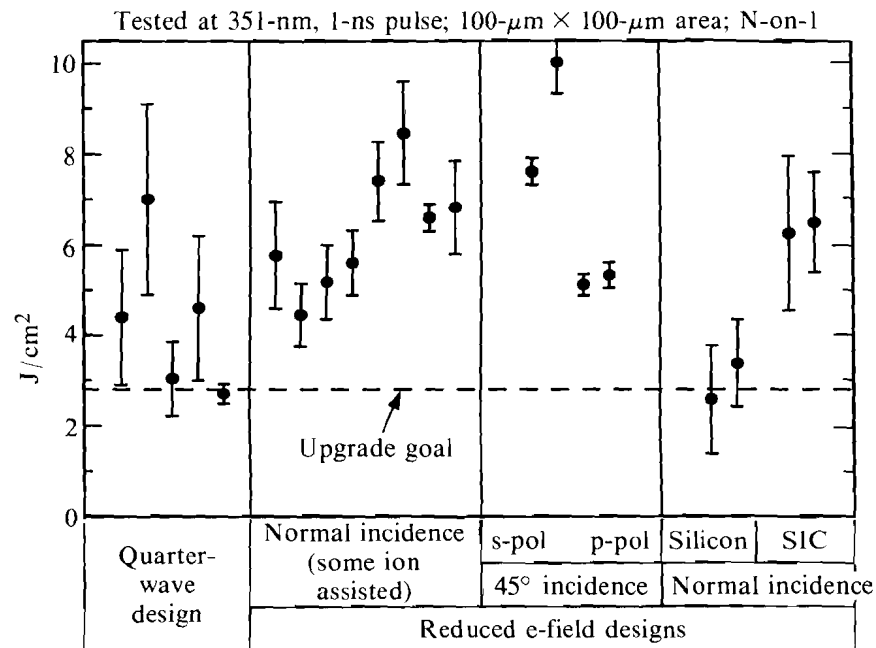
1. Material combinations of $\text{HfO}_2/\text{SiO}_2$, $\text{ZrO}_2/\text{SiO}_2$, and $\text{ZrO}_2/\text{MgF}_2$ had exceeded the Upgrade damage requirement by a significant margin.
2. Designs based on $\text{Sc}_2\text{O}_3/\text{SiO}_2$ had some of the highest thresholds but were deemed too costly to use for all the transport optics.
3. A reduced E -field stack produced the best damage thresholds.
4. An improvement in damage threshold was observed in ion-assisted deposition when using molybdenum grids in a decollimated ion source.

We chose a design based on $\text{HfO}_2/\text{SiO}_2$ for further investigation at high incidence angles because of the higher thresholds of this material pair and the low-UV absorption edge of the hafnia. The damage-threshold data for the $\text{HfO}_2/\text{SiO}_2$ designs at normal incidence exceeded OMEGA Upgrade requirements by a factor of 3 for some samples (Fig. 51.15). These coatings also performed well on silicon-coated silicon carbide substrates, which were considered as a substrate material for the large transport optics. The normal-incidence values exceeded previously published values by a factor of 2 for N -on-1 damage results.

Reduced E -Field Design at Oblique Incidence Angles

High-reflector coatings at normal incidence have shown higher thresholds when designed with suppressed E -field layers at the top of the stack.^{2,3} Absorption at a film defect site will be proportional to the electric-field intensity. Known areas of high absorption, such as interfaces between materials, can be intentionally located at regions of lower electric-field intensity. Usually this means that other low-absorption areas will see a higher electric-field intensity. This trade-off has been used to increase thresholds by a factor of 1.6 for coatings of $\text{Sc}_2\text{O}_3/\text{SiO}_2$.⁴ We have found a similar improvement for coatings at normal incidence. Figure 51.16 illustrates the reason for the improvements. In each frame the time-averaged square of the electric field is plotted within a multilayer (the incident wave arrives from the right). The peak of the standing wave on the right side in the incident media is cut off in these plots, but will be very close to 4 in a high reflector. The first frame [Fig. 51.16(a)] shows the field plotted in the simplest case: a quarter-wave optical thickness stack at normal incidence. The nodes and antinodes of the electric-field intensity are located at the interfaces between the high- and low-index materials. The peak antinodes of the standing wave drop rapidly as the field penetrates the multilayer (a line has been fitted to these

points). The high intensities at the interface are suspect in initiating damage in a high reflector. In the following frame [Fig. 51.16(b)], the thickness of the layers has been modified in the design so that the standing-wave intensity is the same for the top three interfaces of the multilayer (all layers are shown as equal thicknesses in this figure for clarity). The secondary effect is to increase the standing-wave intensity within the homogeneous low-index layer, but, since this layer is composed of a low-absorption material (silica), the overall effect is to increase the damage resistance of the coating. The increase in damage threshold has been documented at normal incidence for mirrors at 351 nm.



G3062

Fig. 51.15
HfO₂/SiO₂ designs have met Upgrade requirements at normal incidence. At a 45° incidence angle differences in the threshold for the two polarizations emerge. The coating thresholds also drop when deposition is on substrates other than glass.

At oblique incidence the E -field must be evaluated separately for s- and p-polarized light. An example of the E -field plot for a 45° unsuppressed reflector is shown in Fig. 51.16(c). Here again the nodes and antinodes are at the interfaces, but now there are two separate plots for the two polarizations. The E -field intensity for the p-polarized light is also discontinuous at the antinodes. If a suppressed E -field coating is designed for normal incidence, it can be “tuned” to operate at an oblique incidence angle by increasing the thickness of all the layers proportionately. The plot for the E -field intensity will then appear as in Fig. 51.16(d). Here neither the s- nor the p-polarized intensity at the interfaces is level, but instead the s-polarized component decreases and the p-polarized component increases in the first three layers of the coating (this design only modified the top two antinodal interfaces). A level E -field design can be attained for one, but not both, polarizations by substituting the appropriate effective index in the original equations supplied by Apfel.³ Instead of using the index n_i for a given material, substitute

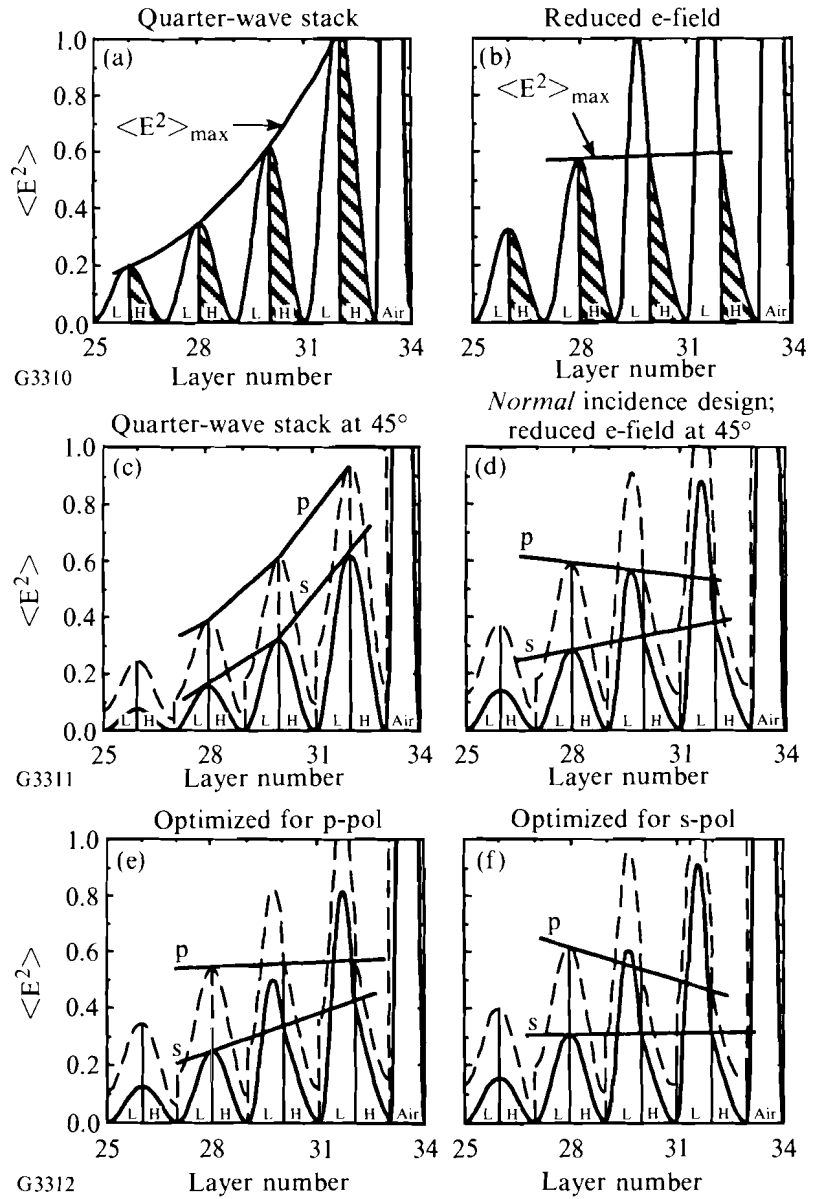


Fig. 51.16

The electric-field standing wave in a thin-film stack can be altered to improve the damage threshold. Each frame shows a plot of the top layers in a stack with the time-averaged square of the electric-field magnitude superimposed over the layers. The H and the L represent high- and low-refractive index layers. A line connects the peak magnitude at the interfaces where high absorption levels could lead to damage. The different frames show the E -field for different designs, incidence angles, and polarization: (a) normal incidence, unaltered quarter-wave-thickness stack; (b) normal incidence, reduced E -field for top six layers; (c) quarter-wave-thickness stack, s- and p-polarization; (d) 45° incidence, reduced E -field for top six layers using normal incidence design; (e) 45° incidence, reduced E -field for top six layers using design optimized for p-polarization; and (f) 45° incidence, reduced E -field for top six layers using design optimized for s-polarization.

$${}^s\eta_i = n_i \cos\theta_i \text{ for the s-polarized case,}$$

$${}^p\eta_i = n_i/\cos\theta_i \text{ for the p-polarized case.}$$

All indices should be converted to the effective index including the incident and substrate. The result is a design optimized for s-polarized light [Fig. 51.16(e)] or a design optimized for p-polarized light [Fig. 51.16(f)]. In the first case, the design for a level E -field intensity in s-polarization produces an E -field intensity increasing with depth for p-polarization. Since thresholds for s-polarization are generally higher than p-polarized threshold, we do not expect this design to be of great utility. The design optimized for p-polarization provides suppressed E -fields at the interfaces in p-polarized light and improves, but does not optimize the E -field intensity for s-polarized light. While an attempt was made to verify these designs experimentally, the results have been obscured by sample variation, as will be discussed in the next section.

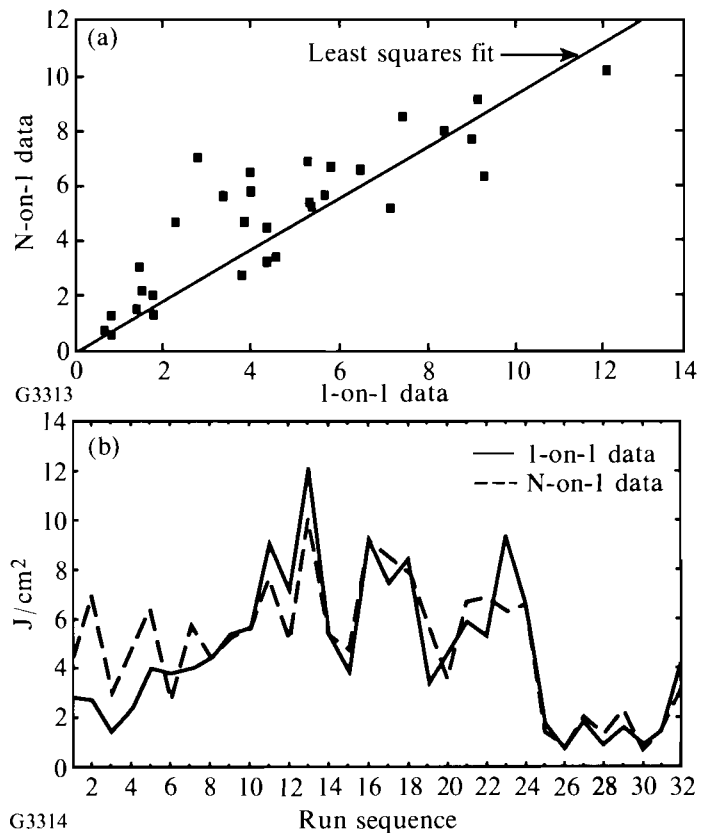
Damage Testing Process for the Oblique Angle Tests

All reflector coatings are tested in the LLE damage-test facility with 351-nm, 0.7-ns, FWHM pulses. Either 1-on-1 or N -on-1 (sometimes both) testing is performed on the samples. In 1-on-1 testing, a new site is chosen for each laser shot. A minimum of ten sites are usually examined. The 1-on-1 damage threshold is defined as the average of the highest nondamaging fluence and the lowest damaging fluence seen in all sites. In N -on-1 testing, one site is subjected to successive laser pulses, each one increasing in fluence above the previous pulse until damage is observed. Three to ten sites are tested in this manner, and the fluences at which damage occurs are averaged to give the N -on-1 damage threshold. N -on-1 testing is more typical of the operation of a large laser facility, demonstrating a hardening effect in the tested surface.⁴ Damage is assumed to have occurred whenever a new scatter site appears within a $100 \times 100 \mu\text{m}$ area observed under dark-field incandescent illumination.

For a restricted coating system, 1-on-1 testing may be used exclusively for comparing and predicting laser damage. In previous years, all samples were subjected to 1-on-1 and N -on-1 testing. While 1-on-1 measurements are faster, N -on-1 measurements more accurately reproduce the behavior of coatings in a multiple-shot laser. Unexpected differences in the two measurements have previously supported taking both measurements when examining widely diverse coatings and optical devices. However, when a single-coating system, the $\text{HfO}_2/\text{SiO}_2$, 351-nm-high reflector was examined, a strong correlation between the 1-on-1 and N -on-1 data was observed. The data from one year of N -on-1 and 1-on-1 tests for the hafnia coating are plotted parametrically in Fig. 51.17(a). A linear fit to the data shown in the figure returns a slope nearing unity. The same data are also plotted against run sequence in Fig. 51.17(b). These data imply that (1) when testing a thin-film multilayer made with tight process controls, the 1-on-1 data are a reasonably good predictor for the N -on-1 data, and (2) there is little indication that a “conditioning” effect occurs with many of these coatings. The absence of conditioning in 351-nm reflectors has also been noticed by investigators at LLNL when examining films using ramped pulses (R -on-1) testing.⁴ Subsequent testing to examine effects of angular sensitivity on the hafnia coatings primarily used 1-on-1 testing to increase throughput.

Fig. 51.17

For a given coating system (same materials, same design) the 1-on-1 damage threshold can accurately predict the N -on-1. In Fig. 51.17(a) the 1-on-1 threshold is plotted against the N -on-1 threshold for a series of hafnia/silica mirrors. A linear fit to this plot has a slope near unity indicating that these films show almost no hardening. In Fig. 51.17(b) a plot of the same data against run sequence shows how closely the two measurements can track each other, thereby reducing the need to make time-consuming N -on-1 measurements.



Previous damage tests indicated that detected thresholds might vary with the time of day, location of test site on the sample, and the environmental condition of the lab. These variations might be a result of equipment warm-up, reliability of the algorithm for determining the peak fluence, sample cleanliness, or changes within the coating itself (aging effects). To test these factors, we used an experimental design approach⁵ that allowed several experimental factors to be tested in one experiment. Five identical substrates were prepared and coated simultaneously with a hafnia reflector tuned for a 60° angle of incidence. A 1-on-1 damage test at 351 nm was performed on each of the four quadrants of the substrate. The four quadrants were tested randomly on different days and at different times during the day. The results [Fig. 51.18(a)] verified that the testing process was giving repeatable results, and most of the measurements showed little variation in either time of day tested, the test date, temperature, lab humidity, or quadrant on the sample. The results did show an unexpected variation among the different samples. These results were surprising, especially in view of the extra effort that went into handling of the substrates. Each substrate was from the same vendor, was cleaned in the same process, and was held in a stainless steel mounting fixture placed in a nitrogen-purged atmosphere after the coating process. Despite these controls on the process, the sample variation dominated the results. The experiment was repeated with a less extensive test sequence to ensure that the results were not caused by an isolated poor coating

run. The second test [shown in Fig. 51.18(b)] shows an even lower threshold with less variation. Both tests indicate that some part of the process introduces variability in the samples, which greatly reduced possible thresholds. The variation of samples coated in the same run indicates that either the deposition process produces a coating that has variable properties across the substrate rack, or the substrate preparation processes are not consistent. The optical uniformity of the substrates is very tightly held by using an elaborate planetary rotation in the system. No measurable quality of the films correlates with the differences in the damage thresholds. These two experiments gave strong evidence that the individual substrates must vary in either the polishing method or the cleaning techniques prior to coating.

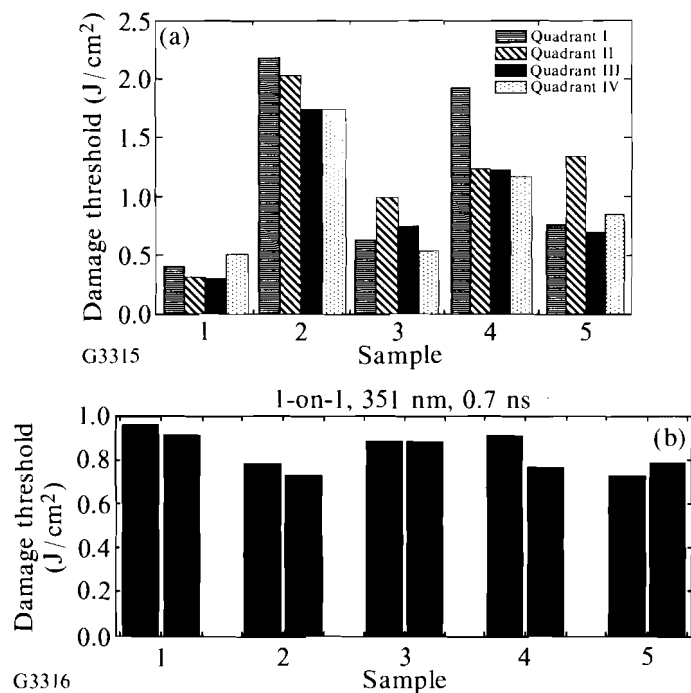


Fig. 51.18

Two experiments were performed to verify repeatability of the testing processes. Samples from the same coating run were tested at different times, days, and sample locations. In Fig. 51.18(a) the samples were tested in four different quadrants, each giving consistent results within each sample and high variation from sample to sample. The results in Fig. 51.18(b) verified the first experiment but with less sample-to-sample variation. Both experiments gave early indications that variations might be caused by substrate preparation.

HR Coatings at High Incidence Angles

The damage threshold drops for most HR coatings when they are examined at incidence angles higher than 40° . A compilation of damage tests at a range of incidence angles for one coating (hafnia/silica) is given in Fig. 51.19. Each of the coatings was tuned to operate at the specified test incidence angle. The decrease in damage threshold tends to be greatest for p-polarized light incident on the substrate. The damage threshold can increase at high incidence angles for s-polarized light in a few isolated tests. The measured damage threshold was found to be sensitive to the damage-test, laser-incidence direction in a number of tested coatings. This observation may appear counter-intuitive since the actual flux density in the plane of the mirror decreases with a higher angle of incidence. It is important to note that the reported damaging fluence at any given angle of

incidence is always defined as the fluence measured in a plane perpendicular to the propagation direction (this is the same plane in which the electric and magnetic vectors lie in the incident media). Actual fluence in the incidence media at the substrate plane may be found by multiplying by $\cos\theta$. It would be expected that this cosine factor would allow the threshold to increase as the incidence angle increases. However, this is not the case with the tested coatings that ranged from 0° to 63° in incidence angles. One reason for this phenomenon is that the Fresnel reflection at all the interfaces drops for p-polarized light and the high-magnitude electric fields penetrate further into the films at the higher angles.

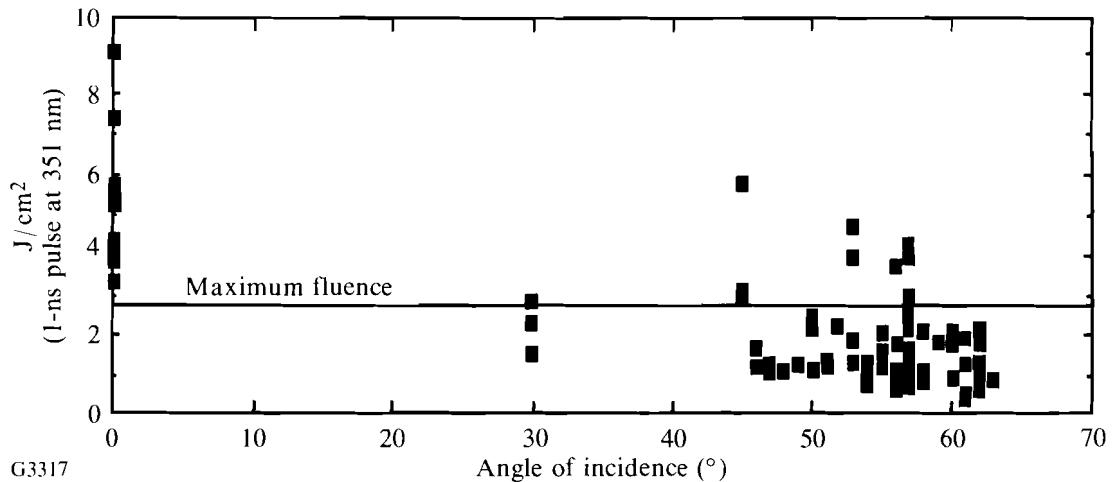


Fig. 51.19

The damage thresholds decrease for the hafnia/silica high reflectors at higher angles of incidence. The thresholds shown are from a series of coatings optimized in reflectance for the test angle and tested with p-polarized light.

A dependence on the test-beam incidence angle was found for some of the HR-coating systems in the study. As the incidence angle increases, the reflectance band for p-polarized light decreases in width. This limits the range in angle over which the mirror will operate. For example, the angular range of high reflectance for a normal-incidence HR will be 0° – 30° while the range for a 55° HR will only be 50° – 59° . If the damage test beam is scanned through this angular range for a given coating, the threshold will drop off precipitously on some samples. An example is given in Table 51.I. This hafnia/silica sample dropped by more than a factor of 2 in damage threshold when the damage-test beam incidence was 3° from the peak reflectance. The corresponding reflectance values varied only a small amount over this range. This effect was seen only in some of the samples.

The variation of damage threshold in the hafnia/silica coatings at oblique angles suggested that further study would determine the main factors for the variation. Some of these coatings had thresholds as high as 5.7 and 4.2 J/cm² for incidence angles of 45° and 53° , respectively. Adequate thresholds were attainable with this material pair but not repeatable. Using experimental design techniques, an experiment was conceived that tested nine different factors in eight separate coating runs using 32 samples (Design of Experiments 2 - DOX2). The factors were all assigned two possible states, as described in Table 51.II.

Table 51.I: Some (but not all) high-reflector coatings experience a sharp drop in damage threshold when tested over a range in angles. The reflectance remains at a high value over the same range.

Angle of Damage Test	1-on-1 Threshold @ 351 nm, 1 ns J/cm ²	Reflectance
51°	1.48±0.08	0.995
53°	4.70±0.02	0.996
55°	4.37±0.30	0.995
57°	1.75±0.01	0.994

G3341

Table 51.II: Factors and values in the DOX2 experiment.

Factor	State 1	State 2
Spatter from <i>e</i> -beam	Low	High
Hafnia starting material	Fully oxidized	Reduced (grey)
Coater operator	Staff A	Staff B
Ion pre-clean	Yes	No
Oxygen	Normal	Ionized
Substrate temperature	150°C	200°C
Reduced <i>E</i> -field design	No	Yes
Substrate	BK7 - Vendor A	Pyrex - Vendor B
Substrate cleaning	Staff C	Staff D

G3342

The surprising result from this experiment is that none of the factors were important predictors of damage threshold, even though the factors had been picked because they had previously exhibited an effect in other experiments. The average threshold of the samples in DOX2 is 1.43 J/cm² with a standard deviation of 0.52 J/cm². As with the DOX1, the prevailing variation was caused by noise apparently from sample to sample. The only factor that might have an effect is the use of reduced *E*-field, but even this factor is of questionable statistical significance. In the best case, using the same process as DOX2, 95% of the future thresholds are expected to be in the range 1.7±0.9 J/cm² in the best case. After DOX2 results, it was clear that some factor in the preparation of the samples before coating was causing significant variation in the samples.

The effects from a wealth of processing steps for the substrate could be eliminated by cleanly cleaving the glass. A cleaved surface will also not require cleaning prior to coating. Typically, polished substrates are scrubbed with a fine polishing compound and a detergent, washed and rinsed in high-purity water, and air dried in a class-10 environment prior to placement in the coating chamber. However, past researchers have had difficulty obtaining a cleave without also creating residue from the fracturing process.⁶ We found that an excellent cleave may be obtained by use of a microtome knife cutter.⁷ Using this device, we were able to produce featureless cleaves in float glass and BK7 glass (Pyrex and fused silica did not cleave well). The cleave showed no particles when observed under dark-field microscopy and was comparable to the cleanest damage-test substrates we have seen.

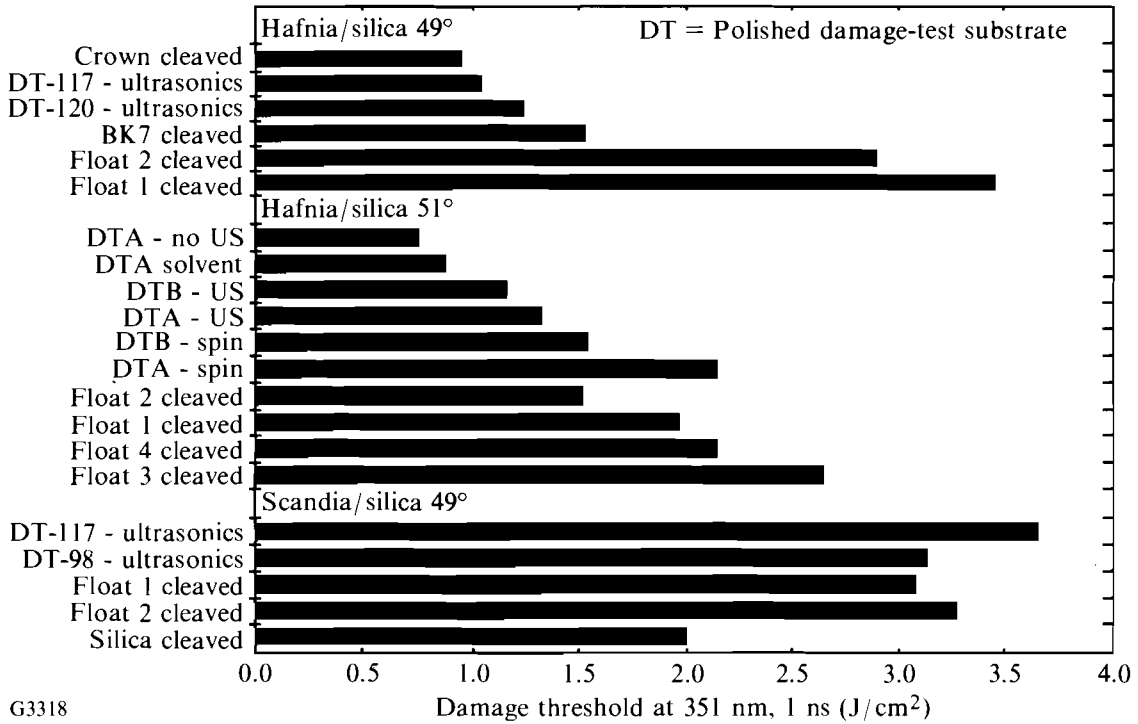
A set of test runs were made with both cleaved and polished glass in the substrate holders. The first run, a hafnia/silica HR at 48°, tested with threshold significantly higher on cleaved float glass than the polished damage test substrates (Fig. 51.20). Two other types of glass, BK7 and a crown glass, showed thresholds as low as the polished pieces. In a second test, seen in the bottom half of Fig. 51.20, various methods of cleaning the damage-test substrate were compared to cleaved samples. These tests indicate that the ultrasonic wash part of the cleaning cycle may be related to the low-damage threshold. Parts cleaned without ultrasonics and dried by spinning had thresholds comparable to or better than the cleaved float. These results fully support the previous results that found sample-to-sample variation was dominant. A discussion of how substrate contamination might affect damage threshold is included.

Scandium Oxide

The scandium oxide/silicon dioxide material pair has provided high thresholds at normal incidence in both LLNL⁴ and LLE² studies. We examined the characteristics of several oblique incidence coatings made from scandia and compared them to normal incidence coatings (Fig. 51.21). While all these coatings meet the damage requirements, they do show the drop in threshold as the incidence angle increases (p-polarization). The few results here do not have as strong a correlation between 1-on-1 and *N*-on-1 threshold as the hafnia results; but the *N*-on-1 results are always higher than the 1-on-1 results, which is caused by the well-known “conditioning” effect seen for some coatings.

The sensitivity of threshold to test incidence angle was exhibited by a 57° scandia reflector. A coating tested at 55°, 57°, and 59° gave 1-on-1 thresholds of 1.7, 3.2, and 2.2, respectively. Once again the acceptable angular range is much lower than would be expected from reflectivity curves. The scandia/silica coatings are less sensitive to substrate contamination than the hafnia coatings. A coating made simultaneously on cleaved and polished substrates produced very small differences in damage threshold (Fig. 51.20, bottom).

Scandia’s promising results make it a good candidate for coating transport optics, although a major drawback is the cost of the material. The 12 kg required to coat all the transport optics would be a major, and possibly prohibitive, cost for the OMEGA Upgrade. Most of the spent material in the deposition chamber could be reprocessed to limit material cost in these runs, but a supplier would



G3318

Fig. 51.20

A cleaved glass surface provides an excellent control surface to study the effects of substrate preparation. Several type of surfaces were coated simultaneously and the damage tested at the stated incidence angle with p-polarized light. The damage test substrates (DT, A and B designate vendors) were cleaned in an aqueous process with either drying by spinning or with ultrasonics and drying in air. The soda-lime float glass produced the cleanest cleaves and also gave the highest thresholds for the hafnia/silica reflectors. The thresholds of scandia/silica reflectors were less dependent on the substrate condition.

have to be found who could hot press the material into a form well suited for e-beam deposition.

Defects and Damage at Oblique Incidence

The predominant finding in this study is the decrease in damage threshold with increasing incidence angle despite the $1/\cos\theta$ geometric fluence dilution. The variation in threshold within samples suggests a defect-driven damage mechanism. Boyer *et al.*⁸ state that the damage threshold fluence for a series of mirrors at 248 nm also decreased for p-polarization. They proposed a model of cylindrical defects oriented normal to the surface in the film, which would expose a greater surface area to the beam at high incidence angles. This proposal, while plausible, does not provide an explanation for the steep drop in thresholds for p-polarized light we have seen in all our samples, nor does it give an explanation for the sensitivity to angular and substrate-contamination effects.⁹ The authors point out that absorption in the multilayers may explain the simple fluence dependence at 248 nm.

The films produced for this study have two predominant types of defects, nodular¹⁰ and spatter. The nodular defects usually grow around a small seed ($\sim 0.5 \mu\text{m}$) and in a conical shape, as schematically shown in Fig. 51.22(a). The seeds may be left from a polishing or cleaning process, and they occasionally occur within the growing film itself. The nodule achieves a domed appearance at the top layers with a dimension dependent on total film thickness. The domed

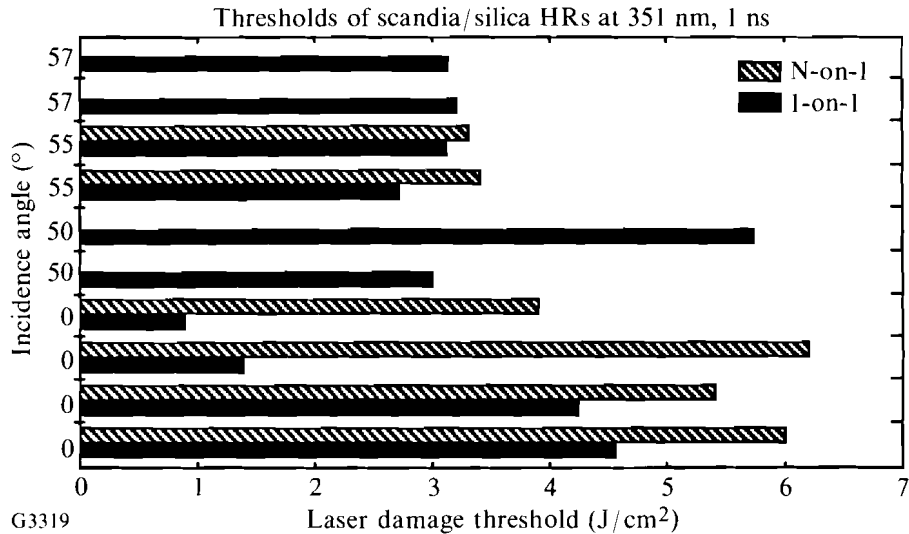


Fig. 51.21 Scandia/silica reflectors maintained high damage thresholds even when tested at high incidence angles with p-polarized light. The scandia reflectors also demonstrated a conditioning effect as shown by the increase of N-on-1 from I-on-1 test results.

top consists of the top layers of the multilayer, which can adequately reflect away any radiation that might otherwise be absorbed by the defect below. Spatter consists of ejected matter from the evaporant melt in the *e*-beam source. Some materials, such as hafnia, tend to reduce to a sub-oxide or metal-rich melt, explosively throwing up copious numbers of particles from the melt. The particles are composed of the sub-oxide melt and range in size from 1 to 10 μm when they arrive at the substrate. The particles are often cylindrical in overall shape and orient with the axis perpendicular to the surface, as seen schematically in Fig. 51.22(b). Figure 51.23(a) shows a scanning electron micrograph of one of these features in a hafnia/ silica film. After forming on the surface, the particle may itself be coated with the remaining multilayer HR coating, as shown in Fig. 51.22(b). Scandia films have very few spatter defects (1 to 2/mm²), while hafnia films show a high density (80 to 150/mm²) of spatter. Both films have an approximate density of nodules of 50/mm².

The spatter defects appear to be responsible for the decrease in threshold of the hafnia film. Figure 51.23(a) shows a SEM view of a spatter on a film after coating. The density of these defects seen in the SEM match the density of the defects seen in dark-field optical microscopy. A different substrate from the same run was exposed to a high-fluence, large-aperture 351-nm beam at an incidence angle of 51°. A scan with the SEM showed only remnant cavities where the spatter had been [Fig. 51.23(b)]. The spatter is protected at normal incidence from the light by a bit of multilayer coating, which covers the top of the defect. At oblique incidence, the light reaches the side of the spatter particle itself where the material is likely to have the same high-absorption characteristics as the melt. (The film itself is evaporated reactively with oxygen to promote reoxidation at the substrate surface.) Thus, the apparent threshold for hafnia may be low; but once the defects have been ablated, the thresholds may be quite high. At present, an investigation is being conducted with a large-aperture beam to test this premise.

Fig. 51.22

The damage mechanism for hafnia films is defect dominated. Two types of defects appear in these films. Figure 51.22(a) shows the nodule defect, which is a growth defect occurring around a submicron seed on the substrate. The domed area at the top of such a defect may produce a range of incidence angles high enough to admit light into the lower regions of the stack. The angles θ_i , θ_f , and θ_n have the values 49° , 75° , and 24° , respectively, in this model. These reflectances of a high-reflector design at these angles are also marked in Fig. 51.24. Figure 51.22(b) shows a rendition of spatter defects from ejected material in the melt. These spatter defects are highly absorbing and will eject when illuminated in oblique incidence. At normal incidence the defect will be protected by a sheath of the multilayer mirror coating.

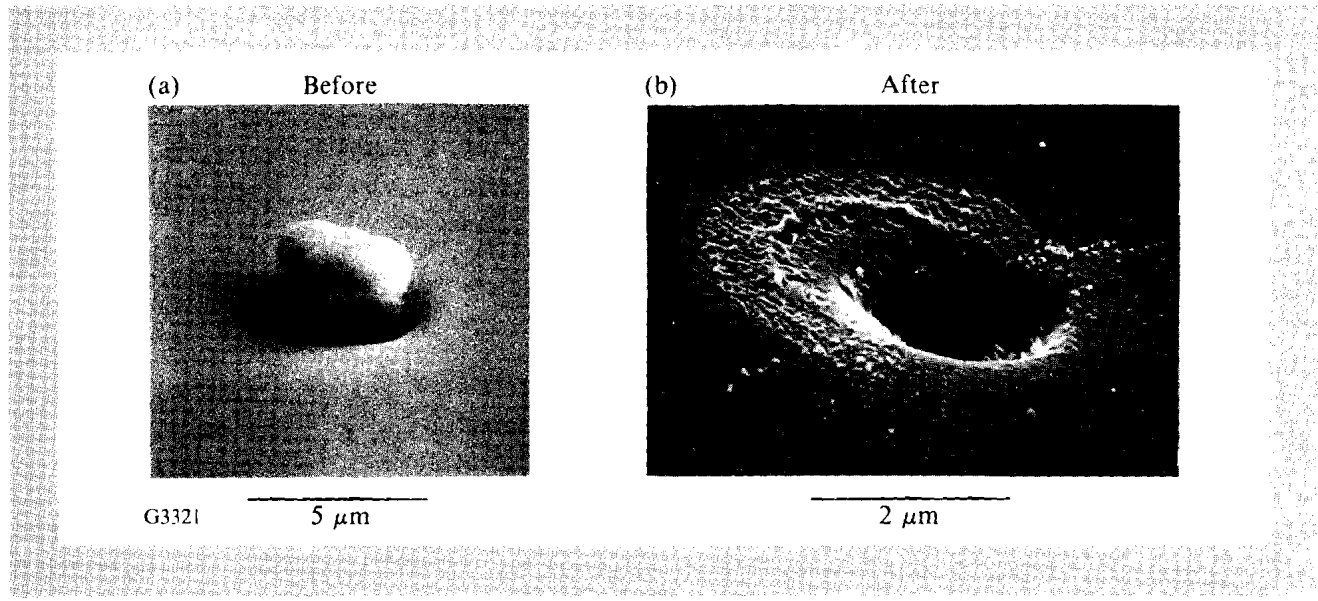
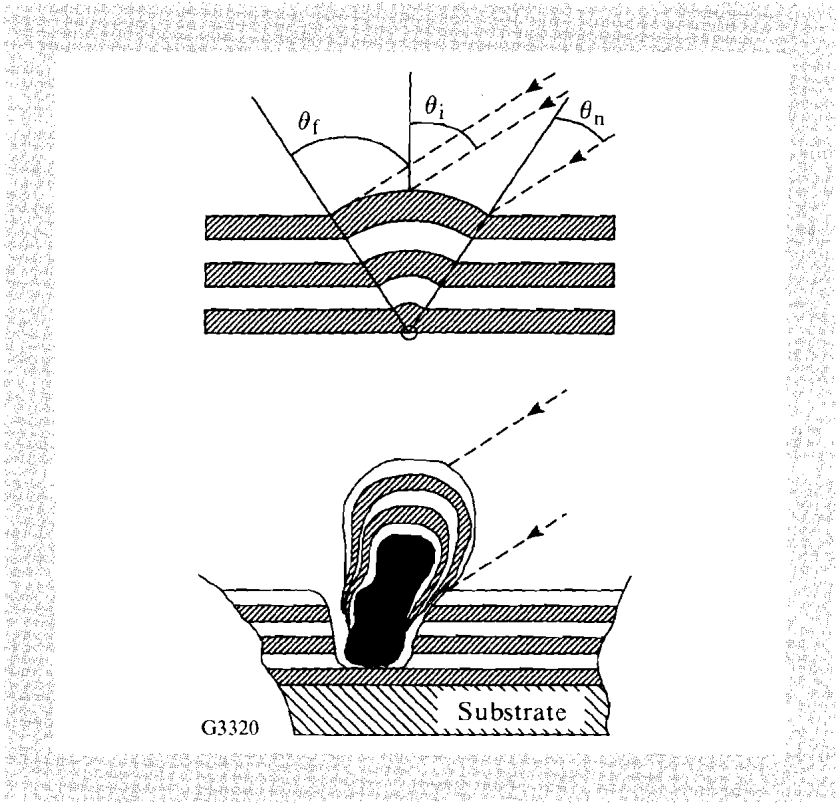


Fig. 51.23

The scanning electron micrographs document the change occurring in a spatter site in a hafnia/silica mirror before and after large-beam testing. An optic examined before exposure shows multiple spatter defects similar to those in Fig. 51.23(a). In Fig. 51.23(b), the defects are seen after exposure to a 351-nm, 1-ns pulse at $>3 \text{ J/cm}^2$. They appear to leave behind a crater after being ejected from the surface. The increased scatter from the crater will be interpreted as damage. The spatter and nodule defects can be distinguished from one another by the size and defect density in the film.

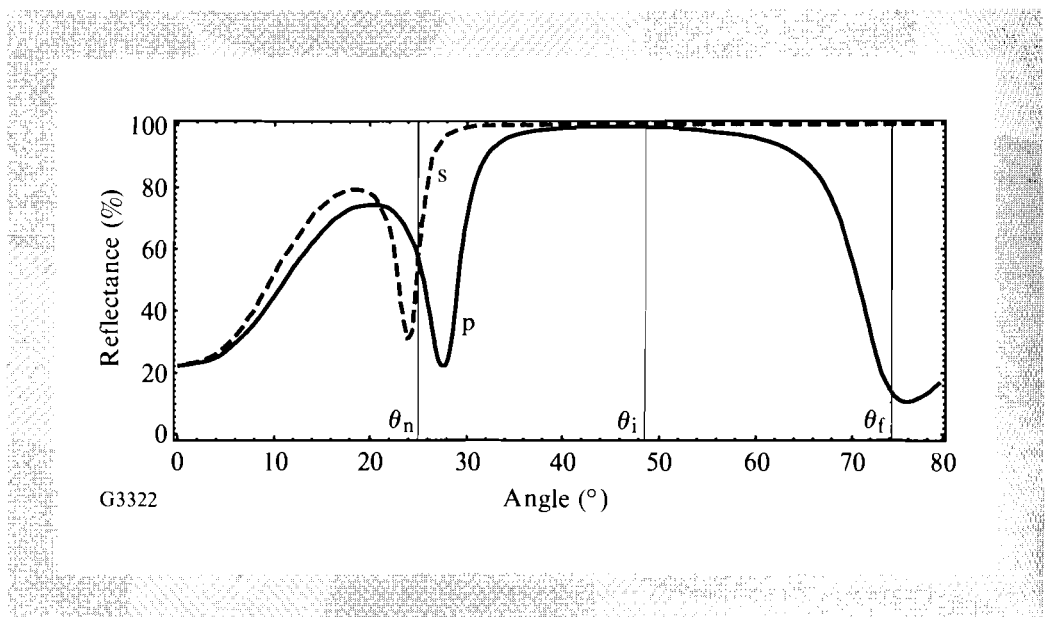
The damage in some of the hafnia and scandia films may be dominated by nodular defect. At oblique incidence, the incident angle at the edge of the defect will be different than the incident angle at the center of the dome [Fig. 51.22(a)]. At near-normal incidence, the change in angle from center to edge will have little effect since the reflection band has a wide bandwidth in θ -space. Two effects predominate at high θ : (1) Since the phase-thickness β of a thin film goes as

$$\beta = \frac{2\pi nd \cos \theta}{\lambda},$$

the phase thickness changes more rapidly at high angle, and (2) as θ increases, the reflection bandwidth decreases for p-polarization. At high incidence angles, the change in θ_n may allow light to pass through to the defect in p-polarization, thereby causing absorption and damage. Since the bandwidth for s-polarized light is much greater, the defect would see less light and be protected from damaging (Fig. 51.24). This effect may be responsible for the incidence-angle sensitivity seen in some of the coatings.

Much of the evidence presented in this article supports this defect-dominated damage model. Hafnia and scandia both have absorption edges near 220 nm and thresholds exceeding 5 J/cm^2 at normal incidence, but hafnia thresholds drop faster at oblique angles. Hafnia produces copious amounts of spatter during *e*-beam deposition. All samples analyzed have shown a distribution of defects in the coating, which probably originated from this spatter. We have found it is possible to reduce the number of defect sites but not to eliminate them entirely. Despite these defects, the hafnia coating may operate well enough if the damage surrounding the ejected spatter site does not propagate. Scandia, which has reasonable damage performance at oblique angles, has a very low spatter rate during deposition and only forms nodules around defects existing on the substrate.

Fig. 51.24
The limited angular acceptance of the dielectric, high-reflector coating may allow damaging radiation to reach defects under a nodule. This plot shows the calculated reflectance for s- and p-polarization for a hafnia/silica high reflector as a function of incident angle. The design peaks in reflectance at 50° for 351-nm light. The angles θ_i , θ_f , and θ_n refer to the incident angles across a nodule in Fig. 51.22(a).



Transport Optic Design for the OMEGA Upgrade

A scandia/silica reflector design would be the best choice for the OMEGA Upgrade transport mirrors, but the cost of materials for all the test and product runs may be prohibitive. Alternatively, the hafnia/silica high reflector should have acceptable performance for low-incidence-angle optics and for high-incidence-angle optics with the electric vector predominantly s-polarized on the optic. Figure 51.25 is a plot of all 120 transport mirrors with incidence angle at the horizontal axis and portion of energy in the s-direction on the vertical axis. The shaded portion represents an area in which all the coatings will be the scandia coating. The input polarization to the target-mirror system can be $\pm 35^\circ$ from the horizontal axis and will be determined by minimizing the number of scandia-based reflectors.

Continued effort will be made to find the criteria for switching to scandia designs. The causes for the large variations in thresholds of the hafnia coating appear to be related to substrate preparation and will be investigated. Alternate methods for depositing hafnia (for instance, from a metal melt with O_2 ion assist) will be considered, as well as methods of recycling the spent scandia. Finally, all the work to date has been with 50-mm-diam test substrates. Tests will be performed on the lightweight transport-mirror material when that design has been finalized and the process technology transferred to the future 72" coating chamber, which will be installed to coat the OMEGA Upgrade optics.

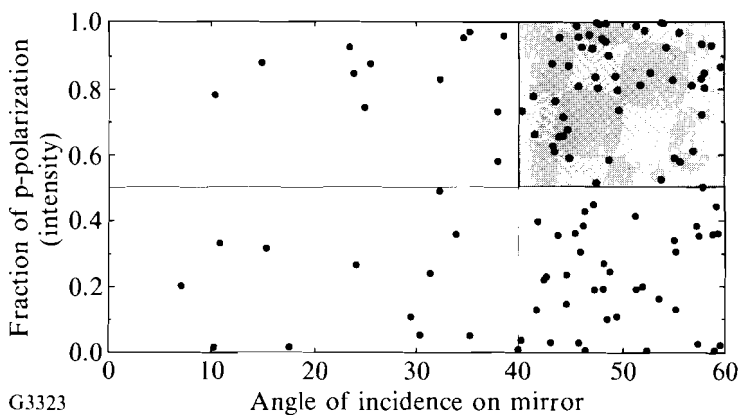


Fig. 51.25
The input polarization is plotted as a function of the incident angle for the transport mirrors in the two-mirror OMEGA Upgrade scheme. The shaded portion represents the mirrors with the highest damage probability and, therefore, those most likely to be coated with the more damage-resistant, scandia/silica, high-reflector coatings.

ACKNOWLEDGMENT

This work was supported by the U.S. Department of Energy Office of Inertial Confinement Fusion under agreement No. DE-FC03-85DP40200 and by the Laser Fusion Feasibility Project at the Laboratory for Laser Energetics, which is sponsored by the New York State Energy Research and Development Authority and the University of Rochester.

REFERENCES

1. LLE Review **44**, 219 (1990).
2. J. H. Apfel, *Appl. Opt.* **16**, 1880 (1977).